Intraseasonal variations and extreme occurrence in the local sea level along the western coast of India remotely controlled by a basin-scale climate variability

Yoko Yamagami[1], Tatsuo Suzuki[1], and Hiroaki Tatebe[2]

[1]Japan Agency for Marine-Earth Science and Technology
[2]JAMSTEC

July 30, 2024

Abstract

The equatorial Kelvin waves, remotely excited by basin-scale climate modes, and subsequent coastal trapped waves significantly influence the intraseasonal variations, their low-frequency modulations, and the frequency of extreme sea level events along the western coast of India. This study demonstrates that the frequency of extreme events are linked to the phase of the Indian Ocean Dipole mode. The temporal changes in the occurrence frequency of extremes are simulated in an eddy-resolving ocean model consistently with observations. However, a non-eddying model significantly underestimate the occurrence frequency of extreme sea level events, suggesting the importance of coastal trapped wave propagations regulated by the horizontal scale with the Rossby radius of deformation. This result implies that many state-of-the-art climate models with a one-degree ocean horizontal resolution may underestimate future coastal sea level variability and the frequency of extreme events under global warming and potential modulations of major internal climate modes.

Intraseasonal variations and extreme occurrence in the local sea level along the western coast of India remotely controlled by a basin-scale climate variability

Y. Yamagami[1], T. Suzuki[1], H. Tatebe[1,2]

[1] Research Center for Environmental Modeling and Application, Japan Agency for Marine-Earth Science and Technology, Yokohama, Japan

[2] Advanced Institute for Marine Ecosystem Change (WPI-AIMEC), Japan Agency for Marine-Earth Science and Technology, Yokohama, Japan

Corresponding author: Yoko Yamagami (y.yamagami@jamstec.go.jp)

† Research Center for Environmental Modeling and Application, Japan Agency for Marine-Earth Science and Technology, 3173-25 Showamachi, Kanazawaku, Yokohama, Kanagawa 236-0001, Japan

Key Points:

- The eddy-resolving model represents the intrasesonal sea level variability along the coast of India explained by coastal trapped waves.
- The occurrence frequency of extreme intraseasonal sea level anomalies is significantly underestimated in the non-eddying model.
- Changes in the probability distributions of sea level associated with the Indian Ocean Dipole are simulated in the eddy-resolving model.

Abstract

The equatorial Kelvin waves, remotely excited by basin-scale climate modes, and subsequent coastal trapped waves significantly influence the intraseasonal variations, their low-frequency modulations, and the frequency of extreme sea level events along the western coast of India. This study demonstrates that the frequency of extreme events are linked to the phase of the Indian Ocean Dipole mode. The temporal changes in the occurrence frequency of extremes are simulated in an eddy-resolving ocean model consistently with observations. However, a non-eddying model significantly underestimate the occurrence frequency of extreme sea level events, suggesting the importance of coastal trapped wave propagations regulated by the horizontal scale with the Rossby radius of deformation. This result implies that many state-of-the-art climate models with a one-degree ocean horizontal resolution may underestimate future coastal sea level variability and the frequency of extreme events under global warming and potential modulations of major internal climate modes.

Plain Language Summary

Sea level variations in the northern Indian Ocean are influenced by ocean waves near the coast, typically in a horizontal scale less than 100 km. It remains unclear whether there is a relationship between extreme events associated with coastal waves and climate variability. Also, if such a relationship exists, it is uncertain how well it is represented in climate simulations, which often have relatively coarse horizontal resolution. To highlight the role of relatively small scale coastal waves, this study compared sea level variations along the western coast of India using two ocean models with coarse and fine horizontal resolutions. We found that the high-resolution model adequately simulates the generation and propagation of coastal waves, and thus successfully simulate sea level variations along western India modulated by large scale climate variability with a 20–150-day time scale. This result suggests that many recent climate simulations may have underestimated the frequency of extreme sea level events in coastal regions.

1 Introduction

The warming climate is projected to cause persistent sea level rise worldwide (IPCC 2022a).

In addition to the global mean sea level rise owing to thermal expansion, melting of glaciers, etc., extreme sea level projections associated with changes in atmospheric circulation and river runoff are also required in coastal regions, especially projections of changes in the occurrence of extreme events (IPCC 2022b). Given that many of the state-of-art climate models in the Coupled Model Intercomparison Project Phase 6 (CMIP6) use a relatively coarse horizontal resolution of approximately 100 km (Tsujino et al., 2020), the projections obtained using these models may underestimate influence of oceanic mesoscale and coastal processes. Hence, it remains unclear whether current sea level projections, particularly in coastal regions, adequately capture changes in extreme sea level events (i.e., as indicated by the tails in probability distributions).

In the densely populated coastal areas of the northern Indian Ocean, projected sea level rises in the Arabian Sea and the Bay of Bengal (Han et al., 2010; Jyoti et al., 2023) present serious risks, including coastal storm surges and extreme tidal events (e.g., Needham et al., 2015). Sea level variability along the coasts of the northern Indian Ocean is strongly influenced by equatorial waves and their resultant coastal trapped wave (CTW). Clarke and Liu (1994) showed that the interannual sea level anomalies (SLA) along the coasts of the northern Indian Ocean were remotely triggered by equatorial zonal winds. More recently, using linear stratified models (McCreary, 1996), several studies have investigated how wind stress forcing over the Arabian Sea, the southern tip of Sri Lanka, and the equatorial Indian Ocean impacts intraseasonal-to-interannual sea level variations along the coast of India (Suresh et al., 2013, 2016, 2018). Wind variations leading to CTWs can be attributed to semiannual basin-scale wind variability that drives the equatorial jet (Yoshida, 1959; Wyrtki, 1973), intraseasonal anomalies associated with the Madden-Julian Oscillation (MJO; Madden & Julian, 1977), and interannual anomalies associated with the Indian Ocean Dipole (IOD) (Saji et al., 1999; Han & Webster, 2002; Aparna et al., 2012).

Although previous studies suggested the potential role of CTWs in the Northern Indian Ocean, the extent to which standard climate models reproduce the coastal sea level variations remains unclear. Therefore, using the coastal sea level variability along the west coast of India as an illustrative example, this study undertakes a comparative analysis of multiple simulations derived from the oceanic component utilized in a climate model. Here we show that an eddy-resolving ocean general circulation model (OGCM) is required to accurately represent sea level variations along the western coast of India. In particular, since intraseasonal sea level variations have a relatively pronounced amplitude and consequently lead to extreme events, this study focuses mainly on how the intraseasonal variations in coastal sea level are represented in OGCMs. Even though the non-eddying OGCM simulation is forced by the same atmospheric boundary conditions as in the eddy-resolving OGCM, the coarse horizontal resolution of the non-eddying OGCM fails to accurately capture the sea level variability, especially variations originating from the equator through the coastal wave guide in the Bay of Bengal.

2 Models, Data, and Methods

This study compares two simulations of CCSR Ocean Component Model (COCO) (Hasumi, 2006); the coarse stand-alone OGCM with a nominal 1° horizontal resolution (COCO-LR) and a global high-resolution version with a horizontal resolution of 0.1° (COCO-HR). Also, to highlight the impact of interannual variations in surface wind forcing on the coastal sea level, we also conducted a sensitivity experiment, referred to as "WIND0". See Text S1 for the details of model setups and validations.

In this study, we used the following observational datasets. PCMDI-SST (Hurrell et al., 2008) was used for the monthly sea surface temperature (SST) data for the period 1993–2019 with a horizontal resolution 1°×1°, as in Tsujino et al. (2020). CMEMS sea level products (DUACS DT2014; Pujol et al., 2016) have a daily interval and a horizontal resolution of 0.25°×0.25° for the period 1993–2019. Drifter-derived monthly climatological surface currents data were also used (Laurindo et al., 2017). To compare sea level anomalies with the satellite altimeter products, we mainly analyzed model outputs after 1993. SLAs relative to global mean was analayzied for both the observation and models.

To examine SLA propagation in the coastal area, we calculated lag composites of SLA for extreme sea level events. A two-tailed *t*-test was adapted to the statistical test at 90% confidence level. To estimate the probability density functions (PDFs) of SLA, Kernel Density estimation was applied (Dehand, 1987; Marshall & Molteni, 1993). A Butterworth filter was employed to isolate the intraseasonal variability within the 20-150 day period.

3 Sea level variance in the Northern Indian Ocean

In this section, we briefly validate the COCO-HR model focusing on sea level variability. COCO-HR showed noticeable improvements in the northern Indian Ocean, especially in regions where oceanic mesoscale eddies are dominant (Fig. 1). In addition to the seasonal variations (Fig. 1a-c, Text S2), COCO-HR more accurately captures detrended interannual and intraseasonal SLAs compared to COCO-LR (Fig. 1d-i). Note that we refer to the 20-150 day band-passed timeseries of detrended anomalies from the daily climatology as “intraseasonal anomalies” hereafter. The noticeable variations in the Somalia-Oman upwelling region are well represented in COCO-HR, aligning closely with observations, although COCO-HR does slightly underestimate them. This difference can be explained that the intraseasonal variability associated with mesoscale eddies and its low-frequency moduration are better represented in COCO-HR under the influence of the Somali Current. Interannual and intraseasonal sea level variability in the western Bay of Bengal also tends to be better represented in COCO-HR, indicating that the intraseasonal variability of coastal trapped waves and local mesoscale variability is also well captured by COCO-HR. These results are also confimed by the spatially high-passed sea level anomalies (Text S2). In the following section, we examined sea level variations along the western coast of India in greater detail.

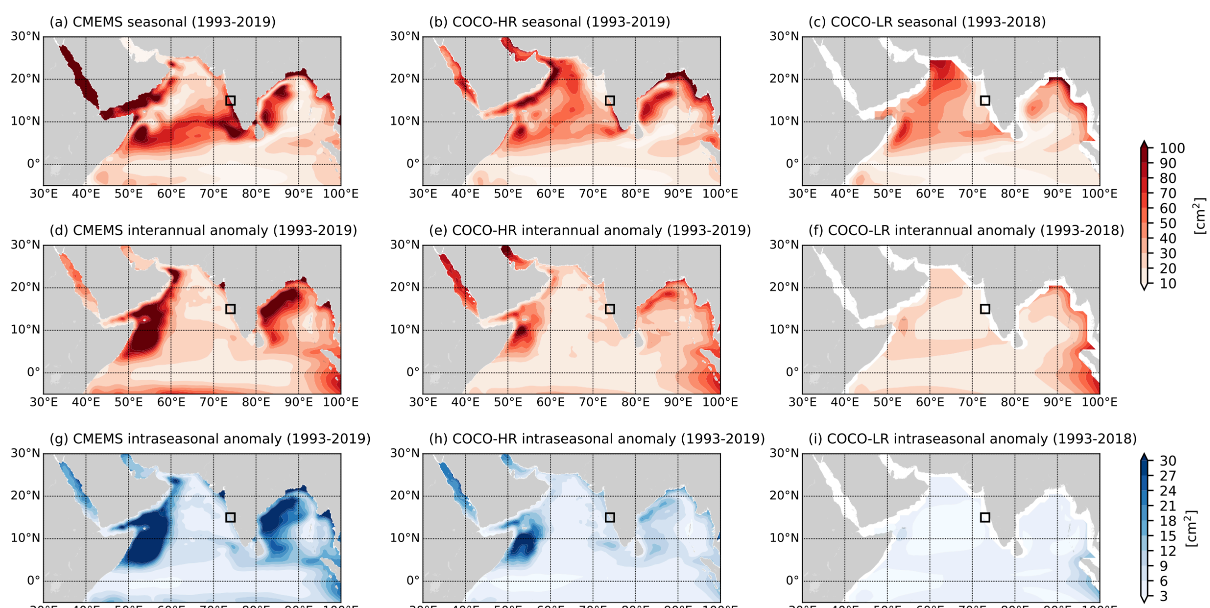

Figure 1. Variances in seasonal sea level anomalies (SLAs) [cm^2] in the northern Indian Ocean for (a) observations, (b) COCO-HR, and (c) COCO-LR. Black boxes indicate the area where area-averaged SLAs are calculated in Section 4 (73°E-75°E, 14°N-16°N for CMEMS and COCO-HR, 72°E-74°E, 14°N-16°N for COCO-LR). (d)-(f) As in (a)-(c), but for interannual SLAs. Interannual anomalies are defined as deviations from the climatology for daily-mean SLAs relative to global-mean. Linear trends are also subtracted. (g)-(i) As in (d)-(f), but for intraseasonal SLAs, which are defined as the 20-150 day band-passed components of interannual SLAs. Note that blue colors and different range of color bars from (a)-(f) are used since variances in intraseasonal SLAs are smaller than those in seasonal or interannual SLAs.

4 SLAs along the western coast of India

4.1 Intraseasonal sea level variations

In order to investigate sea level variations along the western coast of India, area-averaged sea level variations are calculated within 2°×2° boxes at 15°N (black boxes in Fig. 1), ensuring that multiple data points are included in all the boxes. Note that qualitatively similar results are obtained if we use 1°×1° boxes. The comparison indicates that COCO-HR more accurately represents both seasonal (Text S3) and intraseasonal SSH variations along the west coast of India (Fig. 2a-c).

PDFs for 20-150 day band-passed SLA time series are estimated (Fig. 2d,e). In all months, COCO-HR reproduces PDFs that are similar to the observational data, with standard deviations that also match those of the observational data. Conversely, COCO-LR exhibits smaller standard deviations for each PDF compared to the observations, resulting in underestimation of extreme SLA events. Indeed, in observations , the thresholds employed for positive (negative) extreme SLA events, which are defined as events exceeding 95% (5.0%) probability, are estimated to be 4.4 cm (-4.8 cm) (Fig. 2d). For COCO-HR, the occurrence rates of positive (negative) extreme SLA events are 7.3% (4.7%), which is consistent with the observed rates. For COCO-LR, the occurrence of positive (negative) SLA events is 0.95% (0.21%), which is considerably smaller than in the observations. This result means that COCO-LR underestmates the occurrence frequency of the extreme intraseasonal sea level maxima (minima), and underscores the importance of using an eddy-resolving ocean model to accurately hindcast coastal sea level variability.

The narrower PDFs (i.e., indicating less variance) in WIND0 compared to COCO-HR suggests a reduced occurrence of extreme SLA events. Therefore, dynamical wind forcing anomalies are necessary for simulating intraseasonal SLA along the western coast of India (Fig. 2d,e). This result also implies that the contribution of factors other than wind stress forcing, such as buoyancy flux and bartoropic/baroclinic instability associated with West Indian Coastal Current (e.g., Varna et al., 2023), is not predominant. The above result remains qualitatively unchanged if the PDFs are calculated for detrended anomalies without 20–150-day bandpass filtering (Fig. S7). Thus, differences in anomalies with periods shorter (longer) than 20 (150) days do not explain the reduction in the standard deviation of PDFs in WIND0. Consequently, the higher frequency of extreme SLA events in COCO-HR can be attributed to interannual-to-decadal changes in the intraseasonal anomalies. Given that the variance in the intraseasonal component is prominent in both the observation and models (Fig. S8) and contribution of the intraseasonal anomalies to the total amplitude of extreme SLA events is largest in the observation and COCO-HR (Fig. S9), we will discuss the processes driving these differences in PDFs of intraseasonal variability in the next section.

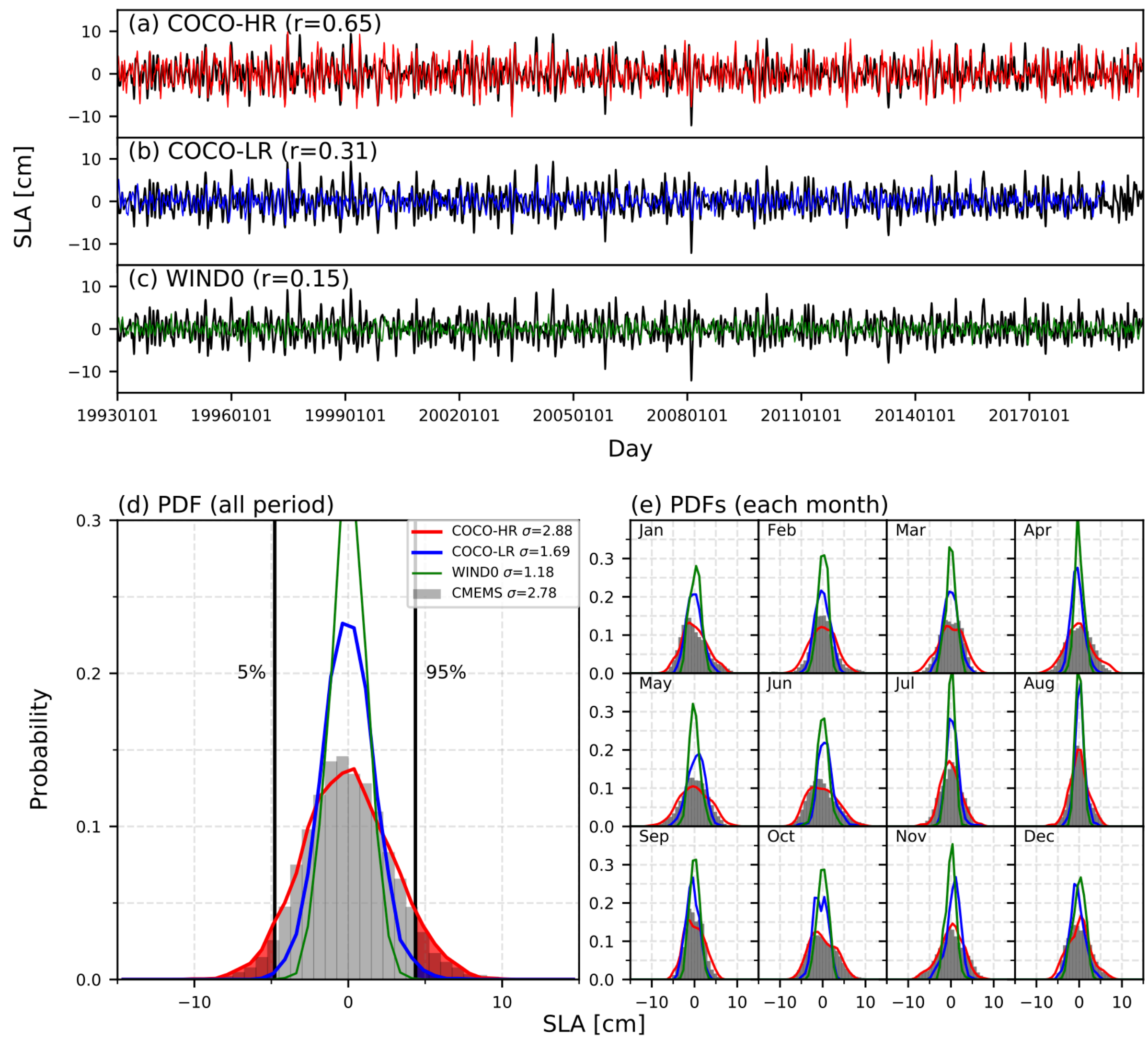

Figure 2. Time series of SLAs [cm] along the western coast of India (15°N; black boxes in Fig. 1) for CMEMS (black), (a) COCO-HR (red), (b) COCO-LR (blue), and (c) WIND0 (green). All panels show time series filtered into band-pass (20-150 days) frequency. The correlation coefficients (r) with CMEMS are shown in panels. (d) Probability density functions (PDFs) of intraseasonal (20-150 days) sea level anomalies (SLA) [cm] along the western coast of India (15°N) for observations (CMEMS; black bars), COCO-HR (red lines), COCO-LR (blue lines), and WIND0 (green lines) for all seasons. PDFs are estimated by kernel density estimation. The standard deviation (σ) for each month is given in the legend. All PDFs are normalized and the vertical axis indicates probability (unit less). Vertical black lines indicate the 5% and 95% anomalies based on CMEMS data. Areas where anomalies exceed the 5 or 95 percentiles for

CMEMS are highlighted in red (COCO-HR) and blue (COCO-LR) colors, respectively, with the corresponding percentile values marked in each model. (e) As in (d), but for each month.

4.2 Resolution dependency of the propagation of coastal trapped waves

Regarding the remote impacts of CTWs on the western coast of India, the large intraseasonal SLA variances in COCO-HR may be attributed to the propagation of sea level anomalies. Figure 3 shows a lag composite of SLA from 0 to 40 days before the occurrence of intraseasonal SLA exceeds +1 standard deviation at the western coast of India (indicated by red symbols in Fig. S8). Since the composites obtained for the negative anomalies are almost mirror images, we discuss only the results obtained for positive SLA events. In the observations, a significant SLA associated with equatorial Kelvin wave is triggered by westerly wind anomalies in the tropical Indian Ocean 40 days prior. Subsequently, this wave reaches the coast of Sumatra island and then propagates as CTWs along the coast of the Bay of Bengal. These waves pass through the southern tip of India, arrive at the western coast of India, and eventually extend into the northern Arabian Sea (Fig. 3a). Furthermore, SLAs also appear to be radiated from the eastern coast of the Bay of Bengal as westward Rossby waves, and are enhanced by easterly wind anomalies along the southern tip of Sri Lanka.

In COCO-HR, similar to the observations, the equatorial Kelvin wave enters the eastern boundary and propagates as CTWs from the Bay of Bengal to the western coast of India (Fig. 3b). Westward SLAs also appeared to be radiated from the eastern coast of the Bay of Bengal to the southern coast of India. On the other hand, COCO-LR does not show SLA propagation in the coastal region from the equator to the Bay of Bengal. Instead, positive SLAs appear to develop locally about 10 days prior, before rapidly increasing in the western coast of India. Previous studies proposed that intraseasonal SLA variations along the western coast of India are predominantly influenced by the propagation of the CTWs from the equatorial Indian Ocean (Suresh et al., 2013). Therefore, the results obtained in this study suggest that COCO-HR effectively captures the propagation of CTWs from the equator. However, the propagation of CTWs from the equator is not well captured by COCO-LR due to the coarser horizontal resolution (Text S4), suggesting an exaggerated influence of local wind and/or thermal forcing in the western coast of India.

In the WIND0 composites, no SLA propagation originating from the equatorial Kelvin waves is evident. This is because the wind stress variations with frequency longer than a year are suppressed in WIND0, and thus interannual modulation of intraseasonal SLAs associated with the equatorial Kelvin waves are not triggered, consequently, the resultant SLA propagation as CTWs in the Bay of Bengal are not generated. Whilst, thermal forcing or mesoscale variability associated with internal oceanic instabilities do not contribute to the intraseasonal SLA propagation. These results are also supported by the lag-composite analysis of SLA from 0 to 40 days following instances when the SLA exceeds +1 standard deviation at the eastern equatorial Indian Ocean (Fig. S10). While both COCO-HR and COCO-LR depict the propagation of equatorial Kelvin waves to the eastern boundary, only the observations and COCO-HR show the subsequent SLA propagation in the Bay of Bengal.

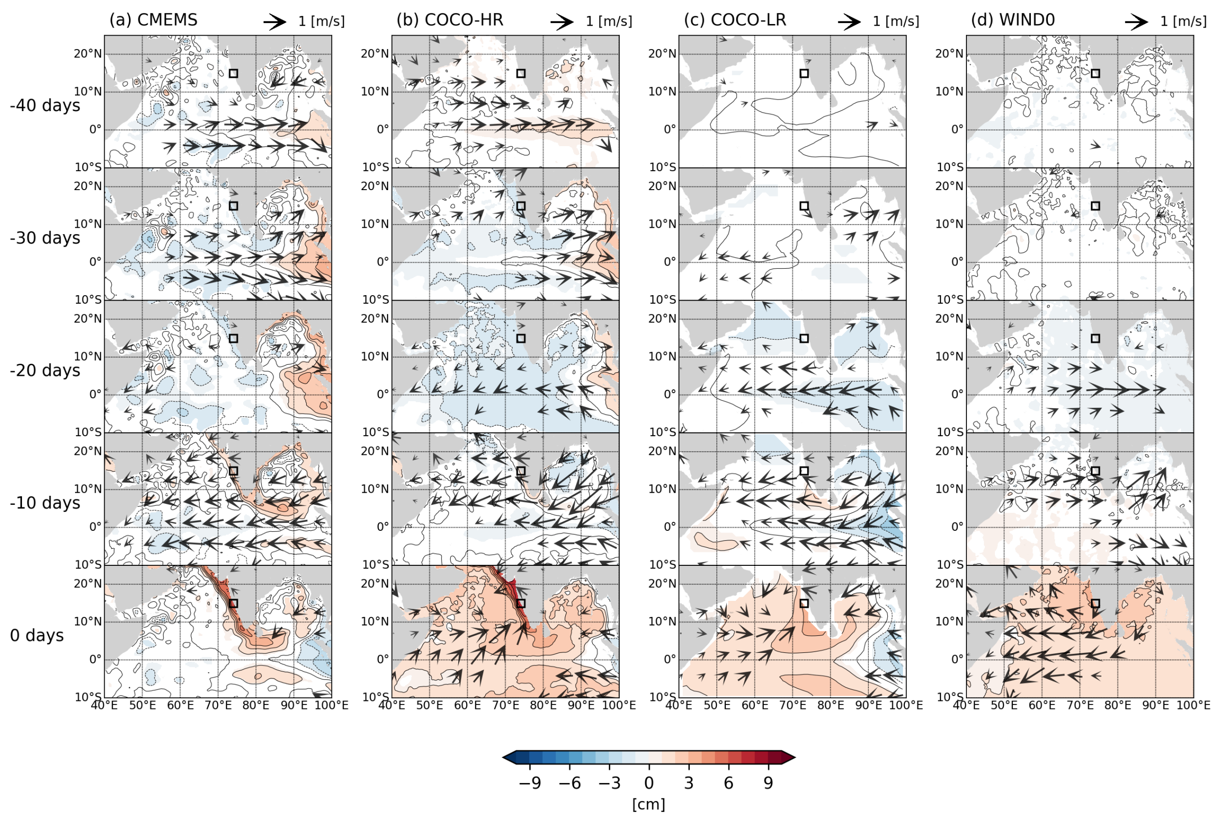

Figure 3. Lag-composites of sea level anomalies (SLA) (contour and color) and 10-m wind (vectors) for area-averaged SLA time series along the western coast of India (black boxes). Data are shown for (a) CMEMS, (b) COCO-HR, (c) COCO-LR, and (d) WIND0. Colors and vectors indicate statistically significant SLA and zonal wind anomalies at the 90% confidence level,

respectively.

4.3 Influence of Indian Ocean Dipole on the probability distribution of coastal SLA along the western coast of India

In section 4.2, differences in PDFs of intraseasonal SLA are attributed to the representation of CTWs. This section examines the origin of the CTWs, particularly their association with wind variations in the tropical Indian Ocean. Given that basin-scale wind anomalies in the tropical Indian Ocean are affected by the IOD, it follows that the IOD contributes to interannual low-frequency SLA variations along the western coast of India through CTWs (e.g., Suresh et al., 2018). However, the extent to which interannual wind anomalies associated with the IOD modulate intraseasonal SLA variations, specifically the probability distribution of coastal SLA along the western coast of India, remains unclear. We therefore investigated the relationship between IOD and intraseasonal SLA, and assessed its representation in both COCO-HR and COCO-LR. In this analysis, the dipole mode index (DMI) is defined as the difference between area-averaged monthly-mean SST difference between the western (50°E-70°E, 10°S-10°N) and eastern (90°E-110°E, 10°S-0°) poles, as defined in previous studies (Saji et al., 1999; Tanizaki et al., 2017). A 3-month running mean is also applied to the DMI. Zonal wind index associated with IOD (Ueq) is also defined as the daily-mean zonal wind are-averaged over 70°E-90°E, 5°S-5°N (Saji et al., 1999) using JRA55-do. Note that the influence of El Niño/Southern Oscillation is less than IOD (figures not shown), which is consistent to the previous studies discussing interannual variations of equatorial thermocline (Rao and Behera, 2005; Yu et al., 2005).

Since SST anomalies associated with the IOD typically peak in October (e.g., Saji et al., 1999), we focus on the relationship between the IOD and intraseasonal SLA along the western coast of India during this month. During positive IOD events, equatorial easterly wind anomalies trigger positive (negative) SLAs along the southern tip of Sri Lanka (in the eastern equatorial Indian Ocean) and, subsequently, positive (negative) CTWs along the western coast of India (coastal region of the Bay of Bengal) as observed (Fig. 4a). The IOD affects the interannual modulation of intraseasonal equatorial zonal wind and SLAs along the western coast of India (Fig. 4d). The correlation between the October-mean of intraseasonal SLAs (Ueq) and the DMI is 0.68 (-0.62), indicating that the IOD modulates the interannual variations in intraseasonal equatorial winds and consequently SLA. During the positive IOD phases, the PDF of the intraseasonal SLA shifts positively (Fig. 4g). Conversely, the PDFs during negative IOD and neutral years are less distinct, which may be related to the asymmetry in the IOD, with negative events having a smaller amplitude than positive events (e.g., Nakazato et al., 2021, An et al., 2023).

COCO-HR can simulate positive SLAs along the west Indian coast during the positive IOD (Fig. 4b). Also, the relatively strong correlation between intraseasonal SLA and DMI (r=0.48) are moderately represented (Fig. 4e), and the PDF shifts positively during positive IOD phases, as observed (Fig. 4h). On the other hand, although the SLA patterns along the west coast of India are similar during the IOD (Fig. 4a-c), intraseasonal SLAs are not correlated with the DMI (r=0.03) and the PDF does not shifts positively in COCO-LR (Fig. 4f, i).

While both COCO-HR and COCO-LR are driven by the same surface forcings, leading to similar large-scale SLA variation patterns in October, there are notable differences at a local scale. This discrepancy is particularly evident when focusing on the local SLA along the western coast of India. COCO-LR underestimates the variability in SLAs associated with intraseasonal variations, and the differences in PDFs of intraseasonal SLAs between the IOD phases are not adequately represented (Fig. 4; Fig. S13). This issue in COCO-LR is likely due to its inability to adequately represent the propagation process of coastal waves originating from the equator, as discussed in the previous section. Therefore, we conclude that interannual wind anomalies associated with the IOD influence the occurrence of extreme SLAs along the western coast of India, and that this effect is represented in the eddy-resolving ocean model. Furthermore, while the non-eddying model can represent the low-frequency SLA patterns associated with the IOD, it lacks the necessary resolution to simulate modulations in extreme intraseasonal SLAs.

Although IOD is mainly characterized by interannual variations, IOD also highly correlates with intraseasonal equatorial wind anomalies and we suggest that influences of IOD on MJO could be implicated (Izumo et al., 2010; Suematsu and Miura, 2018). The large-scale equatorial zonal SST gradient associated with IOD may modulate the characteristics of MJO, potentially driving intraseasonal zonal winds in equatorial Indian Ocean.

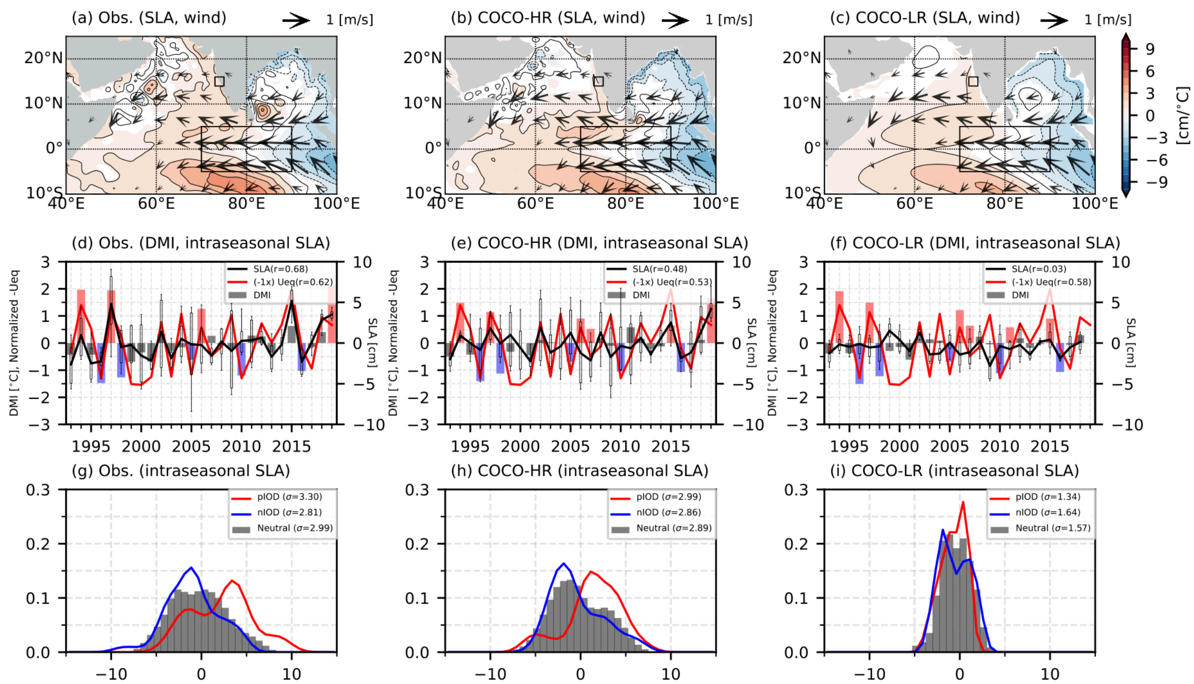

Figure 4. (a) Regressions of October-mean sea level anomalies (SLAs) and 10 m wind anomalies to September-October-November (SON)-mean dipole mode index (DMI) for CMEMS and JRA55-do data. Colors and vectors indicate statistically significant regression coefficients for SLAs and zonal winds at the 90% confidence level, respectively. Black boxes indicate the area where area-averaged SLAs and zonal equatorial wind (Ueq) are calculated, respectively. (d) Time series of the DMI (bar) and intraseasonal (i.e., bandpassed for 20-150 days) SLA along the western Indian coast (15°N; black box in (a)) (black line) and normalized intraseasonal Ueq multiplied by -1 (red line) during October, based on observational data. The correlation between DMI and October-mean intraseasonal SLA is shown in the legend of each graph. Red (blue) bars indicate positive (negative) IOD, while gray bars indicate neutral years. Daily intraseasonal SLAs for a 31-day during October are depicted using box-whisker plots, where boxes span the 25% to 75% ranges in the data, the line indicates the monthly mean, and the whiskers indicate the 5% to 95% ranges in the data. (g) PDFs for intraseasonal SLAs based on observational data for October, as in Fig. 2, but for during positive IOD years (red line), negative IOD years (blue line), and neutral years (gray bars). As in (a), (d), (g), but for (b),(e),(h) COCO-HR and (c),(f),(i) COCO-LR.

5 Summary and discussion

This study showed that the eddy-resolving OGCM (COCO-HR) is capable of reproducing the intraseasonal variability of SLAs along the western coast of India. The results indicate that COCO-HR effectively represents extreme SLA events along the western coast of India. Conversely, the non-eddying model (COCO-LR) significantly underestimate the occurence frequency of these extreme intraseasonal sea level events. In the COCO-HR model, equatorial Kelvin waves originating in the equatorial ocean reach the eastern boundary and subsequently propagate along the coast of the Bay of Bengal and western India, while COCO-LR fails it due to the coarser horizontal resolution. Furthermore, changes in the PDFs of intraseasonal SLAs associated with the IOD are captured only in the COCO-HR model.

This study shows that CTWs are crucial for representing the occurrence of extreme sea level events influenced by basin-scale climate variability, highlighting the importance of representing CTWs in climate models to further improve simulations of coastal sea level extremes. The underestimation of coastal extreme sea level events in the non-eddying OGCM further implies that such extremes may be underestimated in CMIP6 models. For example, the intraseasonal variability along the western coast of India is also underestimated in one of the CMIP6 models (MIROC6) that employs COCO-LR as the ocean component (Fig. S14). Therefore, even when comparisons are made in coupled models, qualitatively similar results can be expected as in this study. Whilst, since evaluating the role of submesoscale eddies is still challenging using global OGCMs, this study should be revisited using OGCMs with the submesocale-resolving resolution.

In the context of recent research on extreme weather events and their links to a warming climate, several studies have emphasized the large-scale drivers of local extreme events (Kawase et al., 2019; Imada et al., 2020). Han et al. (2022) also pointed out the large-scale climate variability drives on local sea level extrems and marine heatwaves in the Indian Ocean. Our results show that the probability of local sea level extremes along the western coast of India is also affected by large-scale wind anomalies associated with the IOD, thus demonstrating a "global-to-local" approach in oceanic contexts. While this study focused on the IOD, future studies should examine the impacts of intraseasonal atmospheric variability, such as the MJO and the Boreal Summer Intraseasonal Oscillation (Wang & Xie, 1997) on coastal SLAs. Consequently, a reassessment of the risk of extreme sea level events, such as storm surges and floods in the coastal areas of the North Indian Ocean, may be needed. This reassessment should focus on the resolution of ocean models to better understand the relationship between changes in local coastal sea level extremes and basin-scale climate variability under global warming.

Acknowledgments

This work was supported by the MEXT program for advanced studies of climate change projection (SENTAN) (Grant Number JPMXD0722680395) and a joint research program between the Ministry of Earth Sciences (MoES) in India and JAMSTEC on ocean downscaling of climate model projections in Indian coastal regions to assess the coastal impact of sea level rise under conditions of global warming. Also, this work was supported by World Premier International Research Center Initiative (WPI), MEXT, Japan. The first author was supported by JSPS KAKENHI Grant Numbers JP20H05729, JP22K14098, and JP22H04487.

Open Research

The altimeter products were produced and distributed by Copernicus Marine Environment Monitoring Service (CMEMS, 2023). Drifter-derived data was downloaded from https://www.aoml.noaa.gov/ftp/phod/pub/lumpkin/drifter_climatology/. JRA55-do data (https://esgf-node.llnl.gov/search/input4mips), PCMDI-SST (https://aims2.llnl.gov/search/input4mips/?institution_id=PCMDI&source_version=1.1.9), COCO-LR outputs (http://esgf-node.llnl.gov/search/cmip6/?mip_era=CMIP6&activity_id=OMIP&institution_id=MIROC&source_id=MIROC6&experiment_id=omip2), and MIROC6 historical simulations (https://aims2.llnl.gov/search?project=CMIP6&activeFacets=%7B%22activity_id%22%3A%22CMIP%22%2C%22source_id%22%3A%22MIROC6%22%2C%22experiment_id%22%3A%22historical%22%2C%22variant_label%22%3A%22r1i1p1f1%22%2C%22variable_id%22%3A%22zos%22%7D) are now distributed through the Earth System Grid Federation. The COCO-HR and WIND0 data have been deposited in the Zenodo (Yamagami et al., 2024).

References

1. Abel, R., Böning, C. W., Greatbatch, R. J., Hewitt, H. T., & Roberts, M. J. (2017). Feedback of mesoscale ocean currents on atmospheric winds in high-resolution coupled models and implications for the forcing of ocean-only models. *Ocean Science Discussions*, *2017*, 1-22. https://doi.org/10.5194/os-2017-24
2. An, S. I., Park, H. J., Kim, S. K., Cai, W., Santoso, A., Kim, D., & Kug, J. S. (2023). Main drivers of Indian Ocean Dipole asymmetry revealed by a simple IOD model. *npj Climate and Atmospheric Science*, *6*(1), 93. https://doi.org/10.1038/s41612-023-00422-2
3. Aparna, S. G., McCreary, J. P., Shankar, D., & Vinayachandran, P. N. (2012). Signatures of Indian Ocean Dipole and El Niño–Southern Oscillation events in sea level variations in the Bay of Bengal. *Journal of Geophysical Research*, 117, C10012. https://doi.org/10.1029/2012JC008055
4. Cheng, X., Xie, S. P., McCreary, J. P., Qi, Y., & Du, Y. (2013). Intraseasonal variability of sea surface height in the Bay of Bengal. *Journal of Geophysical Research: Oceans*, *118*(2), 816-830. https://doi.org/10.1002/jgrc.20075
5. Chelton, D. B., deSzoeke, R. A., Schlax, M. G., Naggar, K. E., & Siwertz, N. (1998). Geographical variability of the first baroclinic Rossby radius of deformation. *Journal of Physical Oceanography, 28*, 433–460, https://doi.org/10.1175/1520-0485(1998)028,0433:GVOTFB.2.0.CO;2.
6. Clarke, A. J., & Liu, X. (1994). Interannual sea level in the northern and eastern Indian Ocean. *Journal of Physical Oceanography*, *24*(6), 1224-1235.
7. CMEMS. (2023). Global Ocean Gridded L 4 Sea Surface Heights & Derived Variables Reprocessed 1993 Ongoing [Data Set]. E.U. Copernicus Marine Service Information (CMEMS). Marine Data Store (MDS). https://doi.org/10.48670/moi-00148
8. Dehnad, K. (1987). Density estimation for statistics and data analysis. Technometrics, 29:4, 495, https://doi.org/10.1080/00401706.1987.10488295
9. Gill, A. E. (1982). *Atmosphere-ocean dynamics.* New York: Academic Press.
10. Gordon, A. L., Sprintall, J., Van Aken, H. M., Susanto, D., Wijffels, S., Molcard, R., et al. (2010). The Indonesian throughflow during 2004–2006 as observed by the INSTANT program. *Dynamics of Atmospheres and Oceans*, 50(2), 115-128. https://doi.org/10.1016/j.dynatmoce.2009.12.002.

11. Han, W., & Webster, P. J. (2002). Forcing mechanisms of sea level interannual variability in the Bay of Bengal. *Journal of Physical Oceanography*, 32(1), 216-239. https://doi.org/10.1175/1520-0485(2002)032<0216:FMOSLI>2.0.CO;2
12. Han, W., Meehl, G. A., Rajagopalan, B., Fasullo, J. T., Hu, A., Lin, J., et al. (2010). Patterns of Indian Ocean sea-level change in a warming climate. *Nature Geoscience*, 3(8), 546-550. https://doi.org/10.1038/ngeo901
13. Han, W., McCreary, J. P., Masumoto, Y., Vialard, J., & Duncan, B. (2011). Basin resonances in the equatorial Indian Ocean. *Journal of Physical Oceanography*, 41(6), 1252-1270. https://doi.org/10.1175/2011JPO4591.1
14. Han, W., Zhang, L., Meehl, G. A., Kido, S., Tozuka, T., Li, Y., et al. (2022). Sea level extremes and compounding marine heatwaves in coastal Indonesia. *Nature Communications*, *13*(1), 6410. https://doi.org/10.1038/s41467-022-34003-3
15. Hasumi, H., 2006: CCSR Ocean Component Model (COCO) version 4.0. *CCSR Technical Report*, 25, 103 pp., https://ccsr.aori.utokyo.ac.jp/;hasumi/COCO/coco4.pdf.
16. Hughes, C. W., Fukumori, I., Griffies, S. M., Huthnance, J. M., Minobe, S., Spence, P., et al. (2019). Sea level and the role of coastal trapped waves in mediating the influence of the open ocean on the coast. *Surveys in Geophysics*, *40*, 1467-1492. https://doi.org/10.1007/s10712-019-09535-x
17. Hurrell, J. W., Hack, J. J., Shea, D., Caron, J. M., & Rosinski, J. (2008). A new sea surface temperature and sea ice boundary dataset for the Community Atmosphere Model. *Journal of Climate*, *21*(19), 5145-5153. https://doi.org/10.1175/2008JCLI2292.1
18. Imada, Y., Kawase, H., Watanabe, M., Arai, M., Shiogama, H., & Takayabu, I. (2020). Advanced risk-based event attribution for heavy regional rainfall events. *npj climate and atmospheric science*, *3*(1), 37. https://doi.org/10.1038/s41612-020-00141-y
19. Intergovernmental Panel on Climate Change (IPCC). (2022a). Sea Level Rise and Implications for Low-Lying Islands, Coasts and Communities. In *The Ocean and Cryosphere in a Changing Climate: Special Report of the Intergovernmental Panel on Climate Change* (pp. 321–446). chapter, Cambridge: Cambridge University Press. https://doi.org/10.1017/9781009157964.006
20. Intergovernmental Panel on Climate Change (IPCC). (2022b). Extremes, Abrupt Changes and Managing Risks. In *The Ocean and Cryosphere in a Changing Climate: Special Report*

of the Intergovernmental Panel on Climate Change (pp. 589–656). Cambridge: Cambridge University Press. https://doi.org/10.1017/9781009157964.008.

21. Izumo, T., Masson, S., Vialard, J., de Boyer Montegut, C., Behera, S. K., Madec, G., et al. (2010). Low and high frequency Madden–Julian oscillations in austral summer: Interannual variations. *Climate dynamics*, *35*, 669-683. https://doi.org/10.1007/s00382-009-0655-z
22. Jyoti, J., Swapna, P., & Krishnan, R. (2023). North Indian Ocean sea level rise in the past and future: The role of climate change and variability. *Global and Planetary Change*, 228, 104205. https://doi.org/10.1016/j.gloplacha.2023.104205
23. Kawase, H., Imada, Y., Sasaki, H., Nakaegawa, T., Murata, A., Nosaka, M., & Takayabu, I. (2019). Contribution of historical global warming to local-scale heavy precipitation in western Japan estimated by large ensemble high-resolution simulations. *Journal of Geophysical Research: Atmospheres*, *124*(12), 6093-6103. https://doi.org/10.1029/2018JD030155
24. Komuro, Y. (2019). *MIROC MIROC6 model output prepared for CMIP6 OMIP omip2*. Version *YYYYMMDD*. Earth System Grid Federation. https://doi.org/10.22033/ESGF/CMIP6.5655
25. Laurindo, L. C., Mariano, A. J., & Lumpkin, R. (2017). An improved near-surface velocity climatology for the global ocean from drifter observations. *Deep Sea Research Part I: Oceanographic Research Papers*, *124*, 73-92. https://doi.org/10.1016/j.dsr.2017.04.009
26. Locarnini, M. M., Mishonov, A. V., Baranova, O. K., Boyer, T. P., Zweng, M. M., Garcia, H. E., et al. (2018). World ocean atlas 2018, volume 1: Temperature. NOAA Atlas NESDIS 81, 52pp. https://archimer.ifremer.fr/doc/00651/76338/
27. Madden, R. A., & Julian, P. R. (1971). Detection of a 40–50 day oscillation in the zonal wind in the tropical Pacific. *Journal of Atmospheric Sciences*, 28(5), 702-708. https://doi.org/10.1175/1520-0469(1971)028%3C0702:DOADOI%3E2.0.CO;2
28. Marshall, J., & Molteni, F. (1993). Toward a dynamical understanding of planetary-scale flow regimes. *Journal of the Atmospheric Sciences*, 50(12), 1792-1818. https://doi.org/10.1175/1520-0469(1993)050%3C1792:TADUOP%3E2.0.CO;2
29. McCreary Jr, J. P., Kundu, P. K., & Molinari, R. L. (1993). A numerical investigation of dynamics, thermodynamics and mixed-layer processes in the Indian Ocean. *Progress in Oceanography*, *31*(3), 181-244. https://doi.org/10.1016/0079-6611(93)90002-U

30. Nakano, H., & Suginohara, N. (2002). Effects of bottom boundary layer parameterization on reproducing deep and bottom waters in a world ocean model. *Journal of Physical Oceanography*, *32*(4), 1209-1227. https://doi.org/10.1175/1520-0485(2002)032%3C1209:EOBBLP%3E2.0.CO;2
31. Nakazato, M., Kido, S., & Tozuka, T. (2021). Mechanisms of asymmetry in sea surface temperature anomalies associated with the Indian Ocean Dipole revealed by closed heat budget. *Scientific Reports*, *11*(1), 22546. https://doi.org/10.1038/s41598-021-01619-2
32. Needham, H. F., Keim, B. D., & Sathiaraj, D. (2015). A review of tropical cyclone‐generated storm surges: Global data sources, observations, and impacts. *Reviews of Geophysics*, *53*(2), 545-591. https://doi.org/10.1002/2014RG000477
33. Pujol, M. I., Faugère, Y., Taburet, G., Dupuy, S., Pelloquin, C., Ablain, M., & Picot, N. (2016). DUACS DT2014: the new multi-mission altimeter data set reprocessed over 20 years. *Ocean Science*, *12*(5), 1067-1090. https://doi.org/10.5194/os-12-1067-2016.
34. Rao, S. A., & Behera, S. K. (2005). Subsurface influence on SST in the tropical Indian Ocean: Structure and interannual variability. *Dynamics of Atmospheres and Oceans*, *39*(1-2), 103-135. https://doi.org/10.1016/j.dynatmoce.2004.10.014
35. Renault, L., Masson, S., Oerder, V., Colas, F., & McWilliams, J. C. (2023). Modulation of the oceanic mesoscale activity by the mesoscale thermal feedback to the atmosphere. *Journal of Physical Oceanography*, *53*(7), 1651-1667. https://doi.org/10.1175/JPO-D-22-0256.1
36. Ridderinkhof, H., Van der Werf, P. M., Ullgren, J. E., Van Aken, H. M., Van Leeuwen, P. J., & de Ruijter, W. P. M. (2010). Seasonal and interannual variability in the Mozambique Channel from moored current observations. *Journal of Geophysical Research: Oceans*, *115*(C6). https://doi.org/10.1029/2009JC005619
37. Saji, N. H., Goswami, B. N., Vinayachandran, P. N., & Yamagata, T. (1999). A dipole mode in the tropical Indian Ocean. *Nature*, *401*(6751), 360-363. https://doi.org/10.1038/43854
38. Suematsu, T., & Miura, H. (2018). Zonal SST difference as a potential environmental factor supporting the longevity of the Madden–Julian oscillation. *Journal of Climate*, *31*(18), 7549-7564. https://doi.org/10.1175/JCLI-D-17-0822.1
39. Suresh, I., Vialard, J., Lengaigne, M., Han, W., McCreary, J., Durand, F., & Muraleedharan, P. M. (2013). Origins of wind-driven intraseasonal sea level variations in the North Indian

Ocean coastal waveguide. *Geophysical Research Letters*, *40*(21), 5740-5744. https://doi.org/10.1002/2013GL058312

40. Suresh, I., Vialard, J., Izumo, T., Lengaigne, M., Han, W., McCreary, J., & Muraleedharan, P. M. (2016). Dominant role of winds near Sri Lanka in driving seasonal sea level variations along the west coast of India. *Geophysical Research Letters*, *43*(13), 7028-7035. https://doi.org/10.1002/2016GL069976.
41. Suresh, I., Vialard, J., Lengaigne, M., Izumo, T., Parvathi, V., & Muraleedharan, P. M. (2018). Sea level interannual variability along the west coast of India. *Geophysical Research Letters*, *45*(22), 12-440. https://doi.org/10.1029/2018GL080972
42. Tanizaki, C., Tozuka, T., Doi, T., & Yamagata, T. (2017). Relative importance of the processes contributing to the development of SST anomalies in the eastern pole of the Indian Ocean Dipole and its implication for predictability. *Climate Dynamics*, *49*, 1289-1304. https://doi.org/10.1007/s00382-016-3382-2
43. Tatebe, H., Ogura, T., Nitta, T., Komuro, Y., Ogochi, K., Takemura, T., et al. (2019). Description and basic evaluation of simulated mean state, internal variability, and climate sensitivity in MIROC6. *Geoscientific Model Development*, *12*(7), 2727-2765. https://doi.org/10.5194/gmd-12-2727-2019
44. Tsujino, H., Urakawa, S., Nakano, H., Small, R. J., Kim, W. M., Yeager, S. G., et al. (2018). JRA-55 based surface dataset for driving ocean–sea-ice models (JRA55-do). *Ocean Modelling*, *130*, 79-139. https://doi.org/10.1016/j.ocemod.2018.07.002
45. Tsujino, H., Urakawa, L. S., Griffies, S. M., Danabasoglu, G., Adcroft, A. J., Amaral, A. E., et al. (2020). Evaluation of global ocean–sea-ice model simulations based on the experimental protocols of the Ocean Model Intercomparison Project phase 2 (OMIP-2). *Geoscientific Model Development*, *13*(8), 3643-3708. https://doi.org/10.5194/gmd-13-3643-2020
46. Varna, M., Jithin, A. K., & Francis, P. A. (2023). Characteristics and dynamics of mesoscale eddies in the eastern Arabian Sea. *Deep Sea Research Part II: Topical Studies in Oceanography*, *207*, 105218. https://doi.org/10.1016/j.dsr2.2022.105218
47. Vinayachandran, P. N., Shankar, D., Kurian, J., Durand, F., & Shenoi, S. S. C. (2007). Arabian Sea mini warm pool and the monsoon onset vortex. *Current Science*, *93*(2), 203–214. http://www.jstor.org/stable/24099306

48. Wang, B., & Xie, X. (1997). A model for the boreal summer intraseasonal oscillation. *Journal of the Atmospheric Sciences*, *54*(1), 72-86. https://doi.org/10.1175/1520-0469(1997)054%3C0072:AMFTBS%3E2.0.CO;2
49. Wyrtki, K. (1973). An equatorial jet in the Indian Ocean. *Science*, *181*(4096), 262-264. https://doi.org/10.1126/science.181.4096.262
50. Yamagami, Y., Suzuki, T., & Tatebe, H. (2024). Data from "Intraseasonal sea level variability along the western coast of India simulated by an eddy-resolving ocean general circulation model" [Data set]. *Zenodo*. https://doi.org/10.5281/zenodo.10633562
51. Yoshida, K. (1960). A Theory of the Cromwell Current (the Equatorial Undercurrent) and of the Equatorial Upwelling. *Journal of the Oceanographical Society of Japan*, *15*(4), 159-170. https://doi.org/10.5928/kaiyou1942.15.159
52. Yu, W., Xiang, B., Liu, L., & Liu, N. (2005). Understanding the origins of interannual thermocline variations in the tropical Indian Ocean. *Geophysical research letters*, *32*(24). https://doi.org/10.1029/2005GL024327
53. Zweng, M. M., Seidov, D., Boyer, T. P., Locarnini, M., Garcia, H. E., Mishonov, A. V., et al. (2019). World ocean atlas 2018, volume 2: Salinity. NOAA Atlas NESDIS 82, 50pp. https://archimer.ifremer.fr/doc/00651/76339/